IEEE Access
Multidisciplinary | Rapid Review | Open Access Journal

Received March 15, 2020, accepted March 31, 2020, date of publication April 6, 2020, date of current version May 11, 2020.

Digital Object Identifier 10.1109/ACCESS.2020.2986021

Double Diffusion Non-Isothermal Thermo-Convective Flow of Couple Stress Micropolar Nanofluid Flow in a Hall MHD Generator System

AUWALU HAMISU USMAN[1,4], USA WANNASINGHA HUMPHRIES[1], POOM KUMAM[1,2,3], (Member, IEEE), ZAHIR SHAH[2], AND PHATIPHAT THOUNTHONG[5], (Senior Member, IEEE)

[1]Department of Mathematics, Faculty of Science, King Mongkut's University of Technology Thonburi (KMUTT), Bangkok 10140, Thailand
[2]Center of Excellence in Theoretical and Computational Science (TaCS-CoE), King Mongkut's University of Technology Thonburi (KMUTT), Bangkok 10140, Thailand
[3]Department of Medical Research, China Medical University Hospital, China Medical University, Taichung 40402, Taiwan
[4]Department of Mathematical Sciences, Bayero University, Kano 700241, Nigeria
[5]Renewable Energy Research Centre, Department of Teacher Training in Electrical Engineering, Faculty of Technical Education, King Mongkut's University of Technology North Bangkok, Bangkok 10800, Thailand

Corresponding authors: Poom Kumam (poom.kum@kmutt.ac.th) and Zahir Shah (zahir.sha@kmutt.ac.th)

This work was supported by the King Mongkut's University of Technology Thonburi, through the ''KMUTT 55th Anniversary Commemorative Fund''. The work of Auwalu Hamisu Usman was supported by the Petchra Pra Jom Klao Doctoral Scholarship for Ph.D. program of King Mongkut's University of Technology Thonburi (KMUTT) and Theoretical and Computational Science (TaCS) Center under Grant 13/2562.

ABSTRACT Nanofluids are potential liquids that enhance the thermophysical characteristics and the ability to transport heat rather than base liquids. This article discusses the non-isothermal heat transfer of the convective steady flow of magnetohydrodynamic micropolar nanofluid over a non-linear extended wall, considering the effects of Brownian motion and thermophoresis, coupled stress, hall current and viscous dissipation effects. Fluid flow is controlled by a high magnetic field. The system of equations is resolved using the Homotopy Analysis Method (HAM) technique and the results are visualized graphically. The effects of different fluid parameters summarizing the problem behavior on primary, secondary and angular velocity, temperature, volume fraction and nanoparticle concentration profiles are measured using graphs. The primary velocity component decreased throughout the entire flow study with magnetic, couple stress and Hall parameters. The large magnetic field parameter and the smaller couple stress parameter lower the secondary velocity, while the increase of the local Grashof number increases the secondary velocity. The strong magnetic parameter, the local Grashof number and the couple stress parameter reduce the angular velocity as observed. The large magnetic parameter, Grashof number, Hall parameter and radiation parameter reduces temperature, while the temperature increases with the increase in Brinkman number and Prandtl number. Brownian motion and thermophoresis encourage the transfer of heat. Tables are used to highlight the impact of dimensionless parameters on the skin friction coefficient, Nusselt and Sherwood numbers.

INDEX TERMS Convective heat transfer, couple stress, hall current, HAM, hall MHD flow, micropolar nanofluid.

NOMENCLATURE

Re	Local Reynolds number
T	Fluid temperature (K)
u, v, w	Velocity components of the dust particles $\left(ms^{-1}\right)$
x, y, z	Coordinate axis
ϕ_w	Wall volume fraction of nanofluid
ϕ_∞	Volume fraction at infinity
T_∞	Temperature at infinity
T_w	Wall temperature
C_w	Wall concentration
C_∞	Concentration at infinity

The associate editor coordinating the review of this manuscript and approving it for publication was Giovanni Angiulli.

Greek Letters:

ξ Similarity variable
ρ Fluid density $\left(Kgm^{-3}\right)$
σ Electrical conductivity $\left(Sm^{-1}\right)$
ρ_p Particle density $\left(Kgm^{-3}\right)$
β_R Mean absorption coefficient

I. INTRODUCTION

A magnetohydrodynamic generator (MHD) is a system that directly generates power by interacting with a rapidly flowing fluid stream, usually ionized gases/plasma. Together with the fluid duct, the very high output current generated by the Faraday flows and reacts with the applied magnetic field resulting in the Hall effect. In other words, the current flowing along with the fluid will result in a loss of energy. Aids with high losses including losses in fluid friction and heat transfer. This loss can be minimized by considering different mass and heat transfer parameters through a mathematical fluid dynamic modeling problem.

Born [1] initially introduced polar fluid notation, which involved resistance to relative rational motion with skew symmetrical stress tensor components. After three decades, linear fundamental equations for polar fluids were developed using the principle statistical mechanics Grade [2]. Cowin [3] and Eringen [4] have advanced some fundamental equations from different perspectives. Micropolar fluids are fluids of the microstructure belongs to a class of non-symmetric stress tensor fluids called polar fluids and, as a special case, includes a well-established classic Navier-Stokes fluid model called ordinary fluids. Eventually, micropolar fluids may consist of fluids made up of rigid, randomly oriented (or spherical) particles restored to a viscous layer where the deformation of the fluid particles is ignored. Eringen [5] has introduced a model of micropolar fluid. As well balanced, it is worth investigating and naming the polar fluid as a micropolar fluid because it was obtained by specializing in its theory of micro fluids. However, it is a well-founded and important generalization of the original Navier-Stokes model, covering several more phenomena than the classical one, in theory and applications. MHD (magnetohydrodynamics) has received considerable interest in renewable energy systems for a wide range of applications involving space travel [6], ocean resources [7], [8], coal-fired power plants [9] and materials processing [10]. Tale systems for Mars missions [11] engineers have developed that the ionization sheath encapsulating the spacecraft can be significantly reduced by generating MHD power, as the intensity (and therefore harmful impact) of the ionization sheath is effectively subdued in key zones as electrons and ions are diverted by the magnetic field and extracted from the electrodes. The redirected energy can be channeled to the engine drive. Because atmospheres usually contain debris and suspensions (cosmic dust), some non-Newtonian effects are present. Consequently, the fluids extracted and used in MHD redirection systems cannot be analyzed as mere Newtonian (Navier-Stokes) viscous fluids. Micro-morphic fluid dynamics or ''micro-fluids'' have been introduced to mimic gyratory movements of suspended particles [10]. The original theory was extremely complex, containing as many balance equations as six times the classical Navier-Stokes theory. Accordingly, Eringen [11] has developed a specialized version of microfluids called micropolar fluids. Such fluids respond to micro-rotational movements and spin inertia, thereby encouraging a couple stress and a distributed object torque that should not be achieved with classic Navier-Stokes equations or viscoelastic flow models. Subsequently, micropolar fluid theory was extended to several branches of rheology including body fluids (blood with corpuscles), paints, colloidal suspensions, liquid crystal suspensions, concentrated silica particle suspensions, oils with very low suspensions, toxic chemical industrial contaminants, lubricants, organic/inorganic hybrid nanocomposites and coastal sediments. Farooq *et al.* [12] dictated a couple of stress effects on the movement of heat in four distinct nanofluid streams. The study of a couple of stress fluids performed by Srinivasacharya *et al.* [13]. They start with a stress parameter that reduces fluid temperature and velocity while increasing concentration. Ramzan *et al.* [14] thought the stretching sheet of the stress fluid flowed above Numerous studies of free convection flows have been published in Umavathi literature on the existence of different geometries [15]. The studies involved Newtonian fluid. However, issues in the petroleum and chemical industries, geohydrology, geothermal energy extraction and medicine include non-Newtonian fluid, fluid flowing through/past porous media. It will be interesting to study the issues of a couple stress fluids that have a technological significance. The flow in the oil reservoirs of the earth can be discussed with the application of the principles of flow through porous media. Atomic power, aeronautics, chemical engineering, free convection problems and space research are emerging, for more details see [16]–[21].

Nanofluid is a type of heat transport medium containing nanoparticles of less than 100 nm which are consistently and continuously dispersed in the base fluid, such as water, oil and ethylene glycol. These dispersed nanoparticles, mostly metal or metal oxide, greatly improve the thermal conductivity of nanofluid, enhance conduction and convection coefficients, considering more heat transport. Dogonchi and Ganji [23] have found MHD nanofluid flow through non-parallel walls. Throughout their research, they focused on the effects of Brownian diffusion and thermophoresis. They found that with the increasing Schmidt number, the concentration and temperature profiles and the Nusselt number increased. Dogonchi *et al.* [24] studied the thermal transfer and the flow of magnetohydrodynamic (MHD) nanofluid between two flat plates when thermal radiation is present. They have shown that the temperature and the Nusselt number are directly related to the fraction of the solid volume, which is inversely related to the radiation parameter. However, they have shown that the coefficient of friction of the skin increases with the increase in the number and expansion ratio of Reynolds. Dogonchi and Ganji [25] Analyzed

nanofluid flow and heat transfer between non-parallel stretch walls with Brownian motion influence. Deduced that the temperature increases with the increase of the heat source parameter and decreases with the increase of the radiation parameter for both the divergent and the converging channels. Dogonchi *et al.* [26] examined the unstable squeezing flow and thermal transfer of MHD nanofluid between infinite parallel plates with an impact on thermal radiation. They have shown that the temperature and the Nusselt number increase with the increase of the radiation parameter. In addition, a number of studies on the impact of nanoparticle use have been published in the research [27]–[36]. Recently, Shah Z *et al.* [37] were studying a couple of stress convection micropolar fluid flow in a hall MHD generator system that focused on the effect of hall current, a couple of stress and magnetic field parameters. Computation of non-isothermal thermo-convection micropolar fluid in a hall MHD generator system with a non-linear distending wall study [38]. However, in the above- literature, studies of the effect of Brownian motion and thermophoresis on MHD micropolar nanofluid flow with a combination of couple stress, hall current and viscous dissipation effects have not been included in the literature. Which appears to be of importance to the application. The present study studied the three-dimensional MHD micropolar nanofluid flow in the presence of magnetic field, over a non-linear extended wall, considering the effects of Brownian motion and thermophoresis, couple stress, hall current and viscous dissipation effects. Together with boundary conditions, the momentum, energy, concentration and volume fraction equations are first transformed into ordinary differential equations and the solution is obtained by using HAM. The velocity, temperature, concentration, and volume fraction profiles are determined and the effects of the different parameters are graphically represented. Skin friction, heat flow and mass transfer values are given in tabular forms for different parameters.

PROBLEMM STATEMENT

Consider the steady three-dimensional non-isothermal thermo-convective flow of couple stress MHD incompressible and electrically conductive micropolar nanofluid and heat transfer in the near-wall MHD Hall generator system. It is known that the wall extends non-linear and concerns the x-axis. The magnetic field B_0 at the y-axis is real. Hall current affects the electrically conductive nanofluid in the presence of a magnetic field. Due to the Hall current, the nanofluid flow changes to three dimensions, increasing the force in the z-direction. All fluid properties are labeled as constant and isotropic. Basic mechanisms, namely Brownian motion and thermophoresis, are considered in the modeling of nanofluid stress couple behavior. On the basis of the above assumption, the mathematical model of the conservation equations for the four field variables, the vector for velocity and temperature as in [37] and concentration (6) (Equation that predicts a change in concentration of diffusing mass at a particle

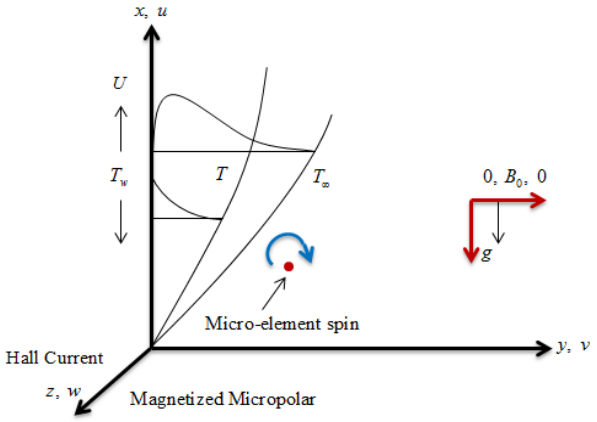

FIGURE 1. Geometric configuration of the micropolar nanofluid flow.

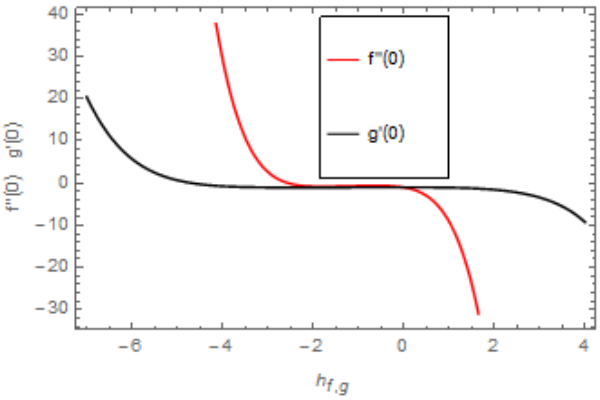

FIGURE 2. h-curves of the $f''(0)$ and $g'(0)$ with 15th-order approximation.

point) and the additional volume fraction (7) for nanoparticles, Described as the volumetric concentration on thermal conductivity of nanoparticles in the fluid [40], is written as follows:

Continuity Equation

$$\frac{\partial v}{\partial y} + \frac{\partial u}{\partial x} = 0, \tag{1}$$

Momentum Equations

$$v\frac{\partial u}{\partial y} + u\frac{\partial u}{\partial x} = \nu\frac{\partial^2 u}{\partial y^2} - \nu'\frac{\partial^4 u}{\partial y^4} - \frac{B_0}{\rho}J_z + K_1\frac{\partial N}{\partial y} + \left[(1-\phi_2)\,\rho_f\begin{pmatrix} B_T\,(T-T_2) + \\ B_C\,(C-C_2)\end{pmatrix} - \left(\left(\rho_p - \rho_f\right)(\phi-\phi_2)\right)\right] g \tag{2}$$

$$v\frac{\partial w}{\partial y} + u\frac{\partial w}{\partial x} = \nu\frac{\partial^2 w}{\partial y^2} - \nu'\frac{\partial^4 w}{\partial y^4} + \frac{B_0}{\rho}J_x, \tag{3}$$

Micro-rotation Equation

$$\frac{G_1}{K_2}\frac{\partial^2 N}{\partial y^2} = 2N + \frac{\partial u}{\partial y}, \tag{4}$$

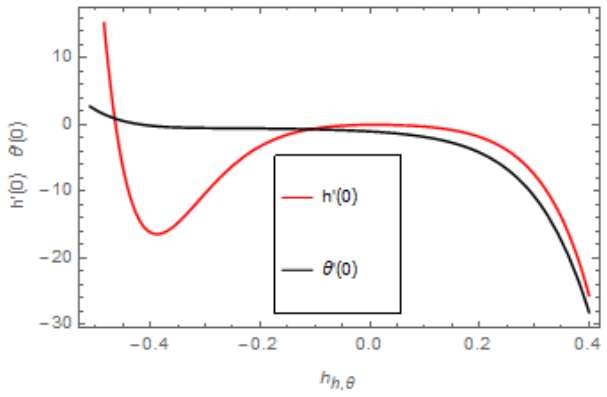

FIGURE 3. h-curves of the $h'(0)$ and $\theta'(0)$ with 15th-order approximation.

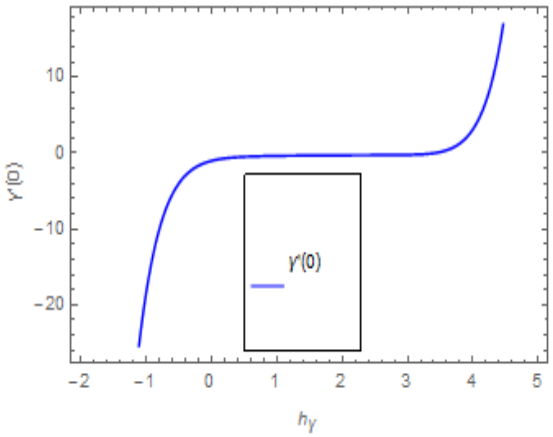

FIGURE 4. h-curves of $\gamma'(0)$ with a 15th-order approximation.

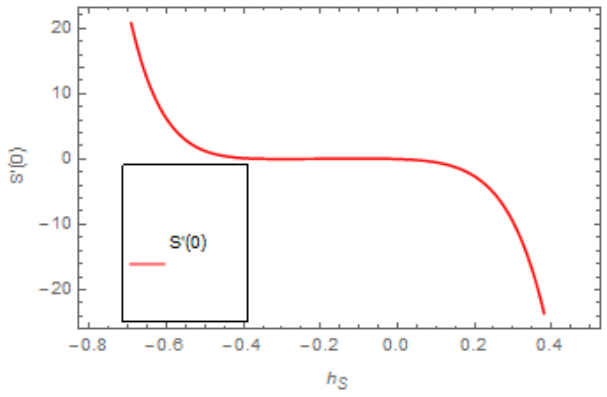

FIGURE 5. h-curves of $S'(0)$ with a 15th- order approximation.

Energy Equation

$$v\frac{\partial T}{\partial y}+u\frac{\partial T}{\partial x}=\frac{\kappa}{\rho c_p}\frac{\partial^2 T}{\partial y^2}+\frac{\sigma\mu_e B_0^2\lambda}{\rho c_p\left(m^2-\lambda^2+1\right)}\left(w^2+u^2\right)+\tau\left[D_B\frac{\partial T}{\partial y}\frac{\partial \phi}{\partial y}+\frac{D_T}{T_m}\left(\frac{\partial T}{\partial y}\right)^2\right]-\frac{1}{\left(\rho c_p\right)_f}\frac{\partial q_r}{\partial y}, \tag{5}$$

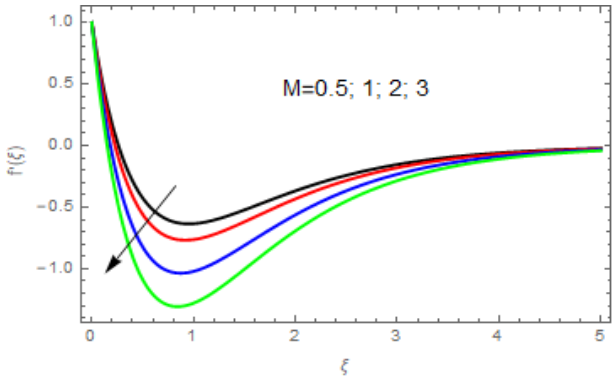

FIGURE 6. Impact of M on $f'(\xi)$.

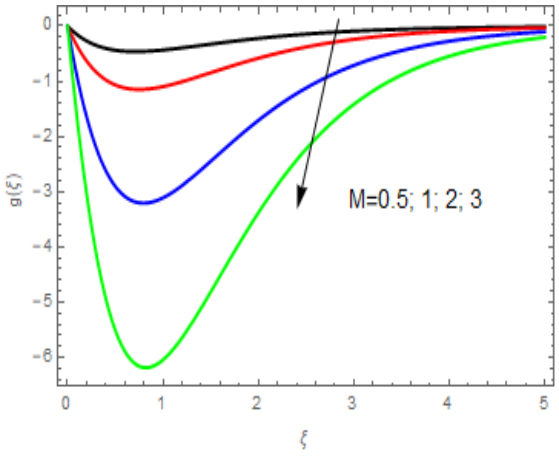

FIGURE 7. Impact of M on $g(\xi)$.

Concentration of the Species Equation

$$V_0\frac{\partial C}{\partial y}=D_m\frac{\partial^2 C}{\partial y^2} \tag{6}$$

Volume Fraction Equation

$$\begin{aligned} V_0\frac{\partial \phi}{\partial y} &= D_B\frac{\partial^2\phi}{\partial y^2}+\frac{D_T}{T_m}\frac{\partial^2 T}{\partial y^2} \qquad (7)\\ u &= U=\mathrm{P}x^n, \quad v=0, w=0, N=0,\\ T &= T_w=T_\infty+Ax^\gamma,\\ \mathrm{C} &= C_w=C_\infty+Ax^\gamma,\\ \phi &= \phi_w=\phi_\infty+Ax^\gamma \quad \text{at } y=0,\\ u &\to 0, \quad w\to 0,\ N\to 0,\ T\to T_\infty,\\ \mathrm{C} &\to C_\infty, \quad \phi\to\phi_\infty \quad \text{at } y\to\infty. \qquad (8) \end{aligned}$$

Agreeing to the Rosseland estimation [22], Ozisik [23] allow the acceptance of the radiation heat flux as

$$q_r=-\frac{4\sigma^*}{3\beta_R}\frac{\partial T^4}{\partial y}=-\frac{4\sigma^* T_2^3}{3\beta_R}\frac{\partial T}{\partial y} \tag{9}$$

where u is the axial velocity, V_0 is the wall injection/suction velocity, C is nanoparticles concentration, T is the temperature of the fluid, T_k The effective thermal conductivity, T_B is the thermal expansion coefficient, C_B is the concentration expansion coefficient, B_0 intensity of the magnetic

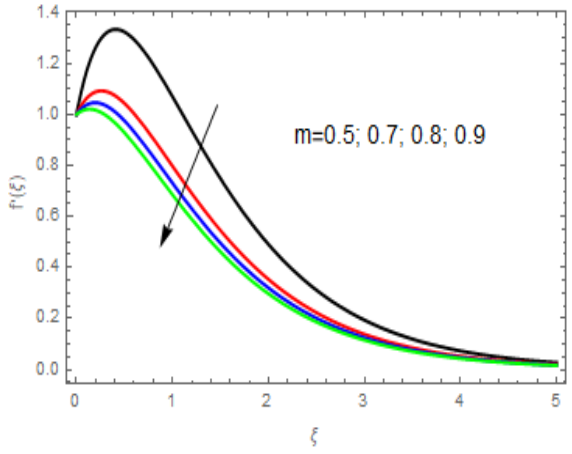

FIGURE 8. Impact of m on $f'(\xi)$.

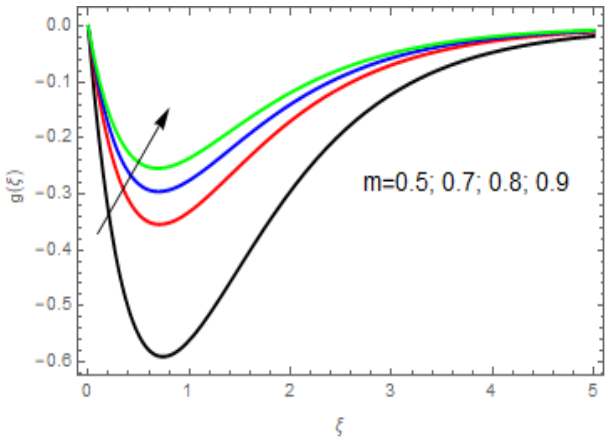

FIGURE 9. Impact of m on $g(\xi)$.

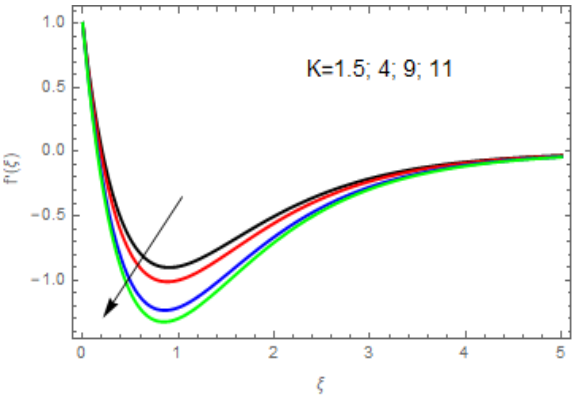

FIGURE 10. Impact of K on $f'(\xi)$.

field, D_B and D_T are the Brownian diffusion coefficient and the thermophoretic diffusion coefficient respectively, β_R is the mean absorption coefficient, σ^* is the Stefan-Boltzman constant, σ is the electrical conductivity, g is the gravitational acceleration, μ is the dynamic viscosity, ρ is the nanofluid density, ρ_p is the particles density, C_p is the specific heat capacity, D_m is the mass diffusivity, τ heat capacity ratio.

The system of equations (2-8) will be transformed from the coordinate system (x, y) to the dimensionless coordinate

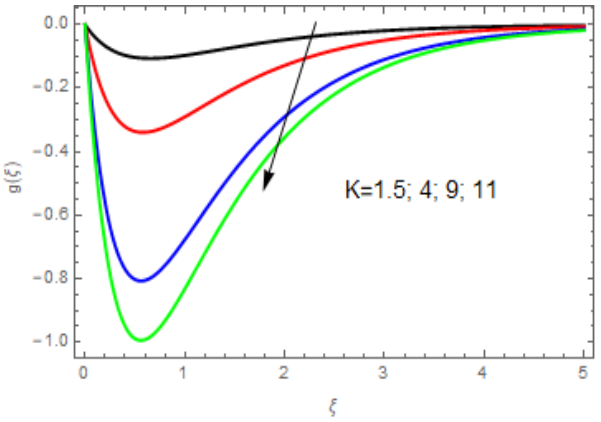

FIGURE 11. Impact of K on $g(\xi)$.

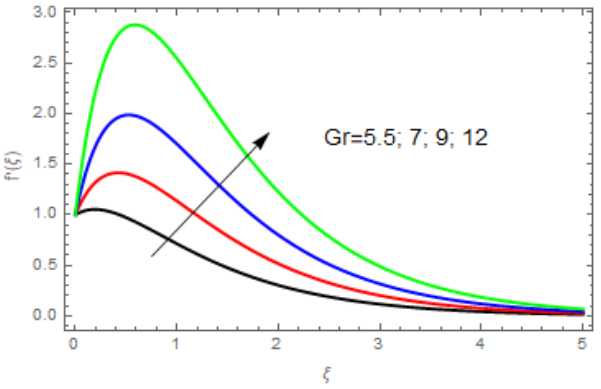

FIGURE 12. Impact of Gr on $f'(\xi)$.

system $\xi(x, y)$, by introducing an appropriate transformation system ($of\ u, T, C, \phi\ to\ f, \theta, \gamma, s$). To transform the coordinate system to a non-dimensional one and this is achieved readily via non-similar transformations, simultaneously eliminating one of the independent variables and reducing the PDEs into ODEs, the following transformation variables are defined.

$$\xi = y\sqrt{\frac{\mathrm{P}(n+1)}{2\nu}}x^{\frac{n-1}{2}}, \quad u = \mathrm{P}x^n f'(\xi),$$

$$v = -\sqrt{\mathrm{P}\nu\left(\frac{n+1}{2}\right)}x^{\frac{n-1}{2}}\left(f + \frac{n-1}{n+1}\xi f'(\xi)\right),$$

$$w = \mathrm{P}x^n g(\xi), \quad N = \mathrm{P}\sqrt{\frac{\mathrm{P}(n+1)}{2\nu}}x^{\frac{3n-1}{2}}h(\xi),$$

$$\theta(\xi) = \frac{T - T_\infty}{T_w - T_\infty}, \quad \gamma(\xi) = \frac{C - C_\infty}{C_w - C_\infty}, \quad s(\xi) = \frac{\phi - \phi_\infty}{\phi_w - \phi_\infty} \tag{10}$$

$$f''' + ff'' - N1h' - \frac{n+1}{2}Kf''''' - \frac{2}{n+1}\left[\begin{matrix} nf'^2 - Gr\theta + GrC\gamma + N_f S \\ + \dfrac{M\lambda}{1+m^2\lambda^2}\left(f' + m\lambda g\right) \end{matrix}\right] = 0 \tag{11}$$

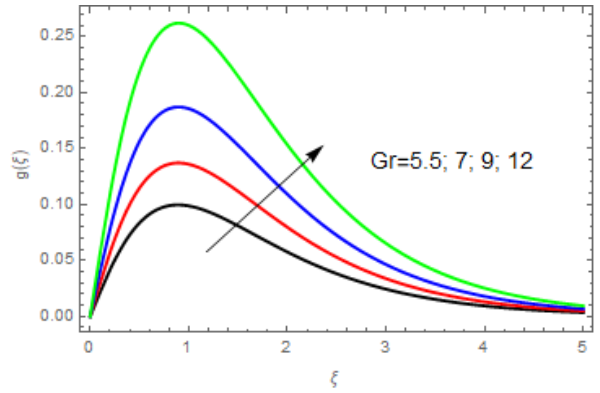

FIGURE 13. Impact of *Gr* on $g(\xi)$.

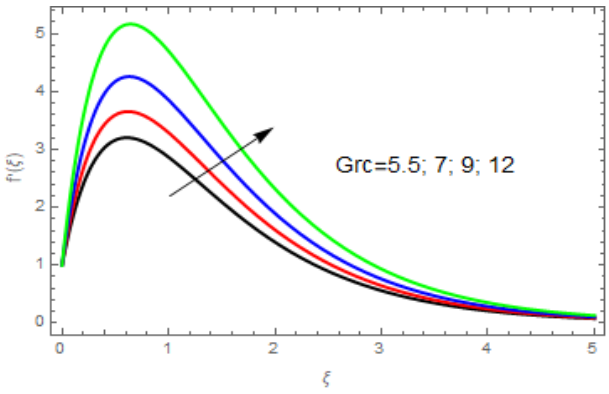

FIGURE 14. Impact of *Grc* on $f'(\xi)$.

$$g'' + fg' - \frac{2}{n+1}\left[nfg' - \frac{M\lambda}{1+m^2\lambda^2}\left(m\lambda f' - g\right)\right] - \frac{n+1}{2}Kg'''' = 0 \tag{12}$$

$$G\left(\frac{n+1}{2}\right)h'' - f'' - 2h = 0 \tag{13}$$

$$Prf\theta' + \theta'' + N_b\theta'S' + N_t\theta'^2 + \frac{2}{n+1}\frac{MBr\lambda}{\left(1+m^2\lambda^2\right)}\left(f'^2 + g^2\right) - \frac{4}{3}R_d\theta'' = 0 \tag{14}$$

$$\left(\frac{2}{n+1}\right)AScy' = (\mathrm{Re})^{\frac{1}{2}}\gamma'' \tag{15}$$

$$\left(\frac{2}{n+1}\right)AScS' = (\mathrm{Re})^{\frac{1}{2}}S'' + \frac{N_t\,(\mathrm{Re})^{\frac{1}{2}}}{N_b}\theta'' \tag{16}$$

With the new boundary conditions given as:

$$f = 0,\quad f' = 1,\ g = 0,\ h = 0,\ \theta = s = \gamma = 1 \text{ at } \xi = 0,$$
$$f' \to 0,\ g \to 0,\ h \to 0,\ \theta = s = \gamma \to 0 \text{ as } \xi \to \infty \tag{17}$$

where ξ is the independent similarity variable, $f(\xi)$ is the dimensionless velocity, $\theta(\xi)$ is the dimensionless temperature, $\gamma(\xi)$ is the dimensionless concentration species and $s(\xi)$ is the dimensionless volume fraction, *Gr* symbolizes the Grashof number, *G* represents micro-rotation parameter, *Re* Reynolds number of injection/rejection, *M* parameter of

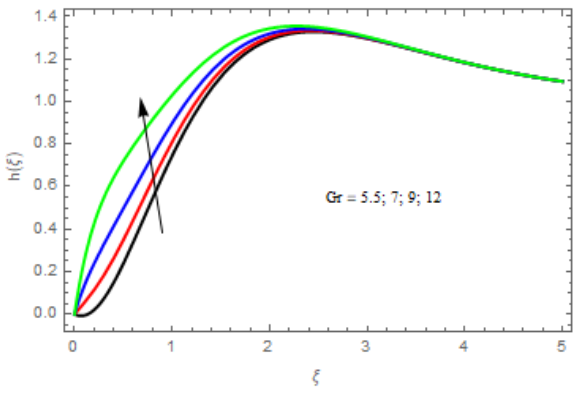

FIGURE 15. Impact of *Gr* on $h(\xi)$.

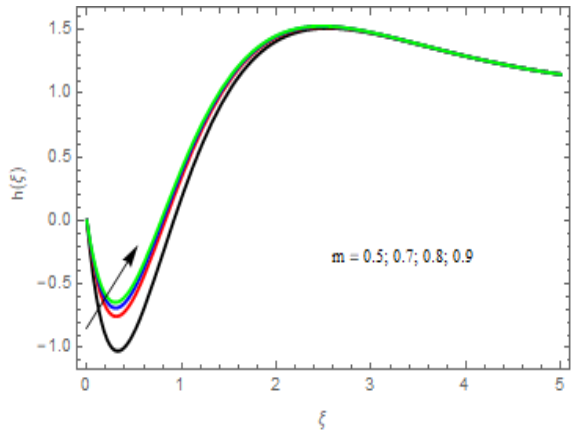

FIGURE 16. Impact of *m* on $h(\xi)$.

the magnetic field, *Pr* Prandtl number, *K* represents the dimensionless couple stress parameter, N_t parameter of thermophoresis, N_b parameter of Brownian motion, *Br* Brinkman number, *Grc* Grashof number thermal and solute, *N*1 characterizes material parameter, A constant, *Sc* Schmidt number, R_d radiation parameter, N_f nanofluid buoyancy ratio.

$$Gr = \frac{B_T(1-\phi_\infty)(T_w - T_\infty)\rho gx}{U^2}, \quad M = \frac{\sigma\mu_e B_0^2 x}{U^2},$$
$$Grc = \frac{B_C(1-\phi_\infty)(T_w - T_\infty)\rho gx}{U^2}, \quad G = \frac{G_1 Px^{n-1}}{k_T\upsilon},$$
$$N_f = \frac{(\rho_p - \rho)(\phi_w - \phi_\infty)gx}{U^2}, \quad N_b = \frac{\tau D_B(\phi_w - \phi_\infty)}{\alpha},$$
$$N_t = \frac{\tau D_T(T_w - T_\infty)}{T_m\alpha}, K = \frac{\nu' Px^{2(n-1)}}{\upsilon^2}, \quad \alpha = \frac{k_T}{\rho C_p}$$
$$Br = \frac{\mu\nu^2}{k_T(T_w T_\infty)}, \quad N1 = \frac{k_1}{\nu}, \ Sc = \frac{V_0}{D_m},$$
$$R_d = \frac{4\sigma^* T_\infty^3}{\beta_R k_T}, \quad A = \sqrt{\frac{(n+1)}{2}}, \ \mathrm{Re} = \frac{Ux}{\nu}. \tag{18}$$

II. PHYSICAL QUANTITIES

For viable applications, the most curiously physical quantities are the coefficient of friction at the canal wall, the rate of heat transfer characterized by the Nusselt number and the rate of mass transfer characterized by the Sherwood number.

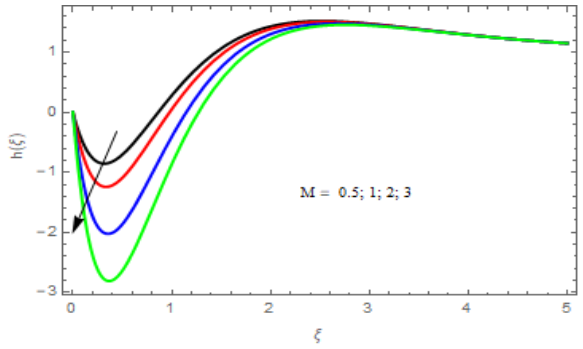

FIGURE 17. Impact of M on $h(\xi)$.

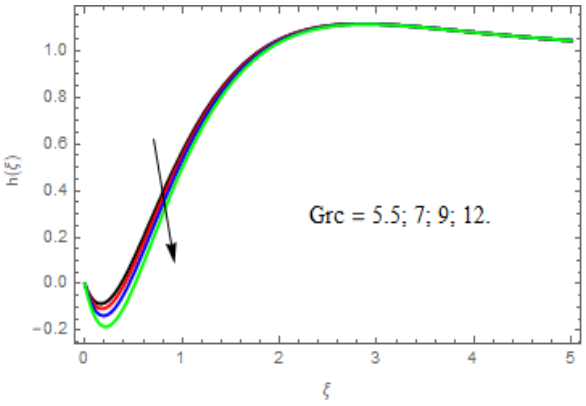

FIGURE 18. Impact of Grc on $h(\xi)$.

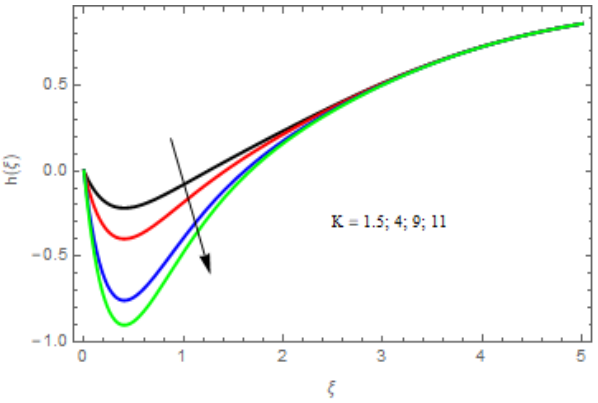

FIGURE 19. Impact of K on $h(\xi)$.

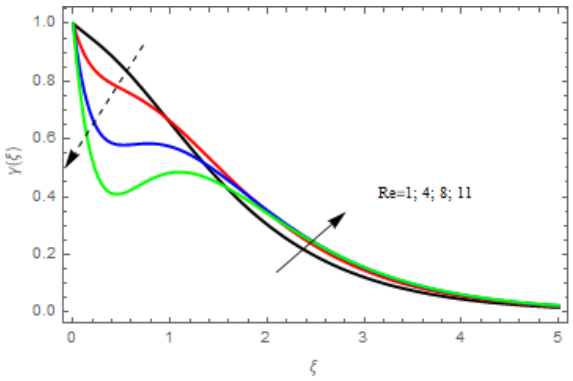

FIGURE 20. Impact of Re on $\gamma(\xi)$.

A. SURFACE DRAG FORCE

Skin friction for primary and secondary velocity components is defined as:

$$\tau_{wx} = \mu \left.\frac{\partial u}{\partial y}\right|_{y=0} = \frac{\mu U}{\sqrt{x}}\sqrt{\left(\frac{U\,(n+1)}{2\nu}\right)} f''(0)\,, \quad (19)$$

$$\tau_{wz} = \mu \left.\frac{\partial w}{\partial y}\right|_{y=0} = \frac{\mu U}{\sqrt{x}}\sqrt{\left(\frac{U\,(n+1)}{2\nu}\right)} g'(0)\,, \quad (20)$$

The coefficients for skin fraction for primary and secondary velocities are given as follows:

$$C_{fx} = \frac{\tau_{wx}}{\frac{1}{2}\rho U^2} = \sqrt{\frac{2\,(n+1)}{\mathrm{Re}}} f''(0)\,, \quad (21)$$

$$C_{fz} = \frac{\tau_{wz}}{\frac{1}{2}\rho U^2} = \sqrt{\frac{2\,(n+1)}{\mathrm{Re}}} g'(0)\,. \quad (22)$$

B. HEAT TRANSFER RATE

The number of the Nusselt number is specified as:

$$Nu = \left.\frac{q_s x}{k_f(T_w - T_\infty)}\right|_{y=0} = -(1+\frac{4}{3}R_d)\sqrt{\frac{\mathrm{Re}\,(n+1)}{2}}\theta',$$

$$q_s = -k\left(1 + \frac{16\sigma^* T_\infty^3}{3\beta_R k_f}\right)\frac{\partial T}{\partial y} \quad (23)$$

C. MASS TRANSFER RATE

The Sherwood number is given

$$Sh = \left.\frac{q_m x}{D_m(C_w - C_\infty)}\right|_{y=0} = -\sqrt{\frac{\mathrm{Re}\,(n+1)}{2}}\gamma,'$$

$$q_m = -D_m\frac{\partial C}{\partial y} \quad (24)$$

III. CONVERGENCES OF HAM

As Liao [39] has determined, the convergence and approximation rate for the HAM solution depends significantly on the auxiliary parameter values. To this end, h-curves are plotted taking h in such a way as to ensure the convergence of solutions [39]. Here to see the admissible values of h, the h-curve is plotted for approximation of 15th order as shown in Figures 2-5, by taking the values of the parameters as: $M = 0.1$; $n = 0.1$; $\lambda = 1.1$; $N_f = 0.3$; $Gr = 0.5$; $K = 0.3$; $\mathrm{Re} = 0.4$; $Grc = 0.1$; $Sc = 0.6$; $A = 0.1$; $m = 1.1$; $N1 = 0.2$; $Br = 0.1$; $\mathrm{Pr} = 0.72$; $N_b = 0.1$; $G1 = 0.5$; $N_t = 0.3$; $R_d = 0.2$. To control and speed up the convergence of the approximation series with the aid of the h-curve, it is important to choose the appropriate value of the auxiliary parameter. The distance for which the- is parallel to the is known as the set of permissible h_f and h values for which the solution sequence converges. These figures show that the ranges for the values h_f and h-axis

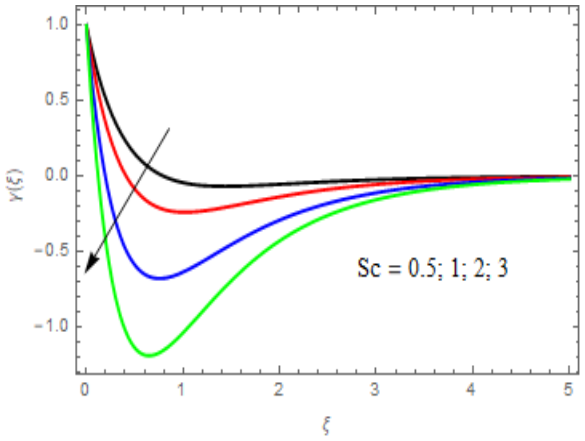

FIGURE 21. Impact of *Sc* on $\gamma(\xi)$.

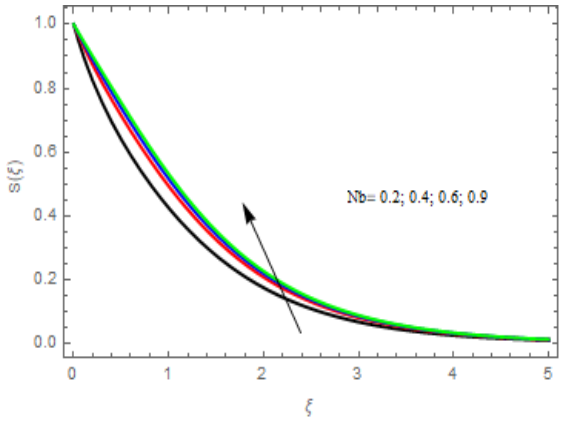

FIGURE 22. Impact of N_b on $s(\xi)$.

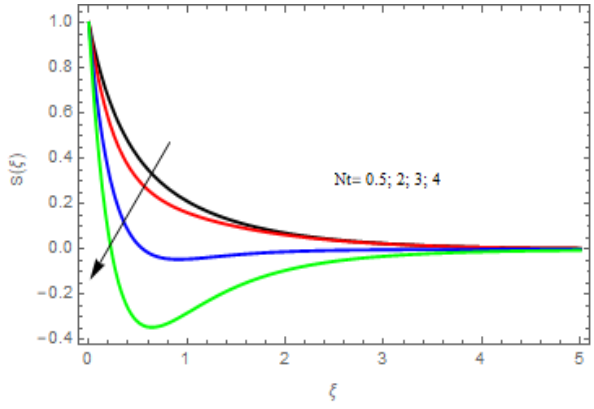

FIGURE 23. Impact of N_t on $s(\xi)$.

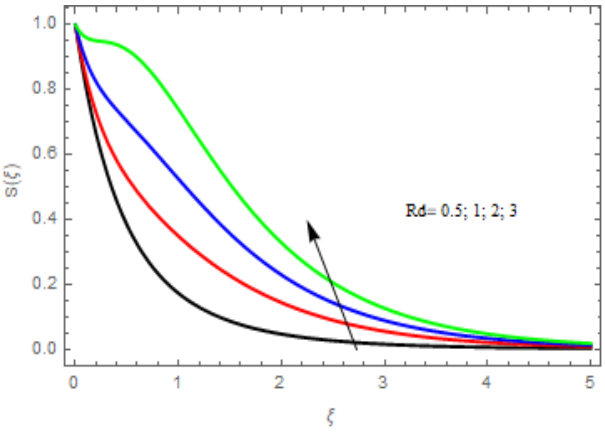

FIGURE 24. Impact of R_d on $s(\xi)$.

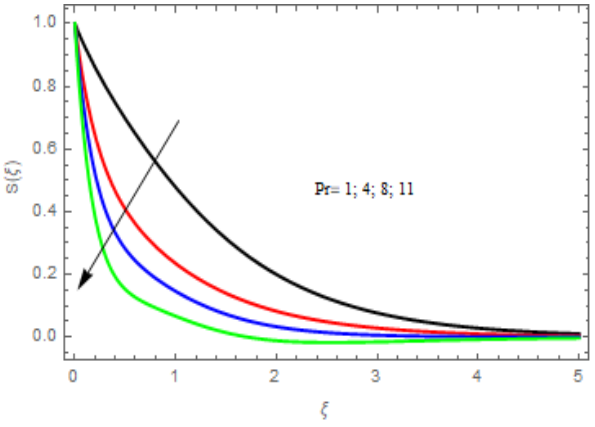

FIGURE 25. Impact of Pr on $s(\xi)$.

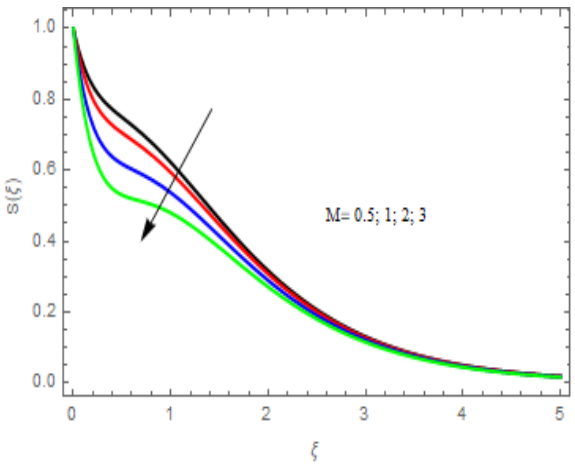

FIGURE 26. Impact of *M* on $S(\xi)$.

are appropriate. $-0.5 \leq h_f \leq 0.20, -0.25 \leq h_g \leq 0.1, -0.1 \leq h_h \leq 0.4, -0.6 \leq h_\theta \leq 0.45, -0.3 \leq h_S \leq 0.0$ and $0.2 \leq h_\gamma \leq 3$.

IV. RESULTS AND DISCUSSION

Figure illustrations uncovered the effect of various parameters on fluid profiles. A noteworthy impact of M on secondary and primary velocity is shown in Figures 6 and 7. For greater M estimation the Lorentz drag force is boosted, which increases the resistance to fluid movement and therefore decreases $f'(\xi)$ and $g(\xi)$, which indicate higher magnetic field has a coordinate effect on the two velocity. Figures 8 and 9 show the impact of m on $f'(\xi)$ and $g(\xi)$ Figure 8 depict the impact of m on $f'(\xi)$. Which reveals that increase in m decelerates the velocity profile $f'(\xi)$ of the wall. Figure 9 disclose the effect of m on $g(\xi)$ The increase in m increases the g in all the flow. The term of the Hall in Eq. (12) is very positive when the magnetic field parameter has positive

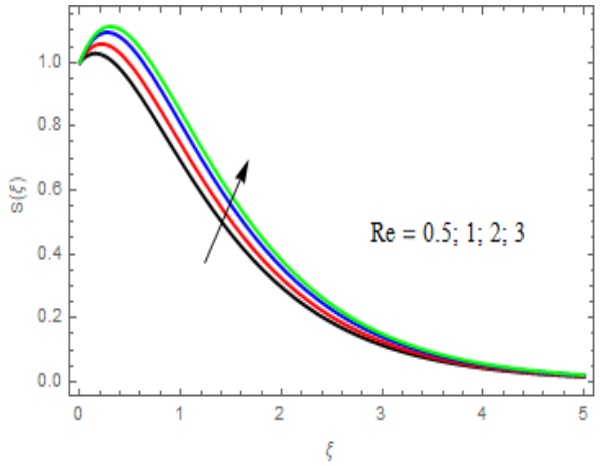

FIGURE 27. Impact of Re on $S(\xi)$.

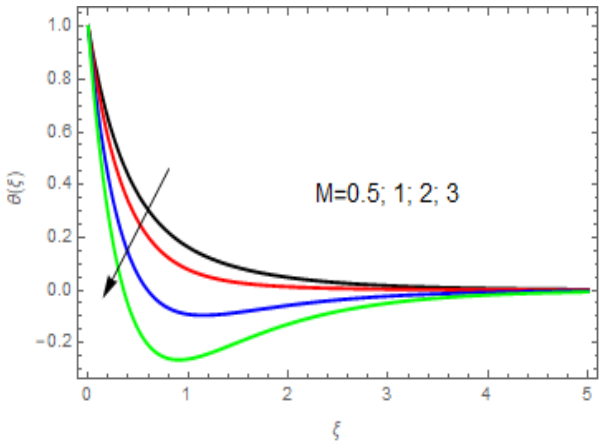

FIGURE 28. Impact of M on $\theta(\xi)$.

values. It does, however, help to back up the cross of the flow and illustrates a remarkable cross stream spurt. The effect of K on $f'(\xi)$ and $g(\xi)$ is shown in Figures 10 and 11, respectively. From both figures, it is observed that the velocity decreases with the K, which shows that, because of the presence of a couple stresses, this happens. Developing a couple stress parameter will make the fluid progressively thick, which will reduce the flow of fluid. Consequently, the acceleration approximations of couple stress parameter decreased the secondary and primary velocity as depicted in Figures 10 and 11. Also, the couple stress parameter is related to fluid movement, and thereafter has no effect on the temperature profile. Effect of Gr on $f'(\xi)$ and $g(\xi)$ shown in Figures 12 and 13, respectively. Here, in Figure 12, the velocity increases with an increase in the Grashof number near the wall. Nevertheless, the current of free conventions reinforces the wall that saved the free flow. A similar effect of Grashof number on secondary velocity is shown in Figure 13. The flow of fluid rises near the wall with a larger value of Grashofs number. For secondary velocity, therefore, the greater proportion of the area is determined in accordance with the primary velocity. Figure 14 shows that the primary velocity increases with the increase in the Grashof of the

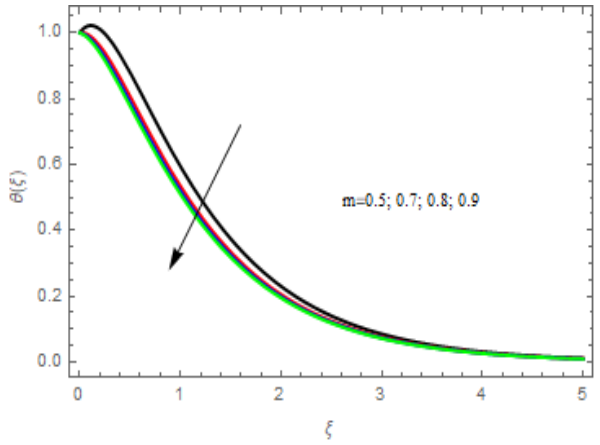

FIGURE 29. Impact of m on $\theta(\xi)$.

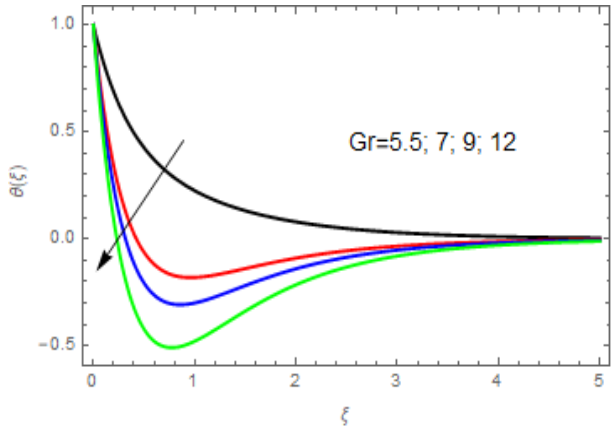

FIGURE 30. Impact of Gr on $\theta(\xi)$.

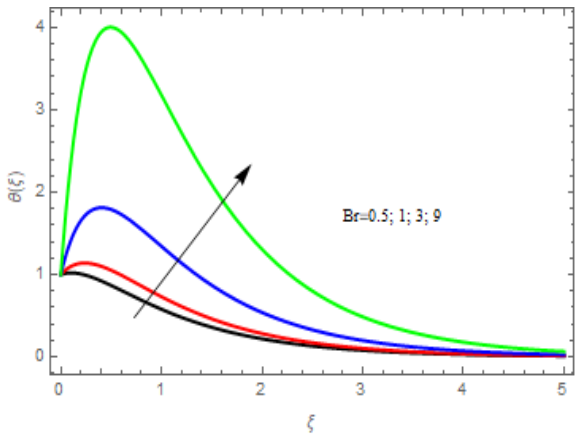

FIGURE 31. Impact of Br on $\theta(\xi)$.

solutal solutal number. More prominent Hartmann number strongly reduced the primary and angular velocity profile of the Lorentz drag force components as shown in equations (11) and (12). The components are negative and positive, which is why the fluid flow is restricted. The acceptance of secondary Lorentz drag force is indeed positive, which is in support of secondary momentum advancement when the magnetic field is positive. These effects are delineated in Figure 6 and 17.

TABLE 1. Influence of M, $N1$, m, λ, Gr, Grc, N_f and K on $f''(0)$.

M	$N1$	m	λ	Gr	Gr_c	Nf	K	$f''(0)$
0.1	0.2	1.1	1.1	0.5	0.1	0.3	0.3	-2.32240
0.3								-2.343597
0.5								-2.364956
	0.3							-2.372776
	0.4							-2.380594
	0.5							-2.388400
		1.2						-2.379888
		1.3						-2.373246
		1.4						-2.367976
			1.2					-2.365234
			1.3					-2.362900
			1.4					-2.360912
				0.6				-2.346756
				0.7				-2.332487
				0.8				-2.318276
					0.2			-2.332487
					0.4			-2.360912
					0.6			-2.389347
						0.4		-2.403550
						0.5		-2.417768
						0.6		-2.431980
							0.4	-2.434285
							0.5	-2.440576
							0.6	-2.444876

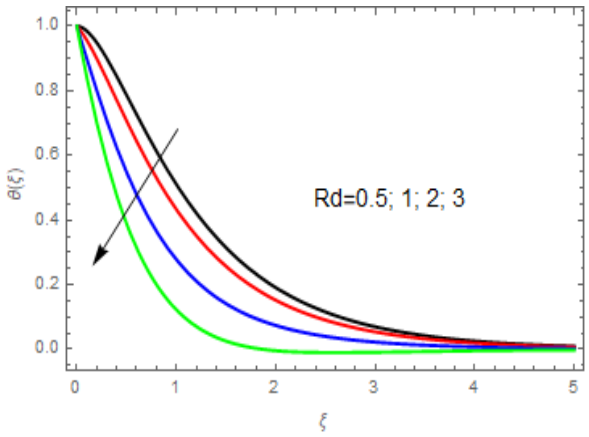

FIGURE 32. Impact of R_d on $\theta(\xi)$.

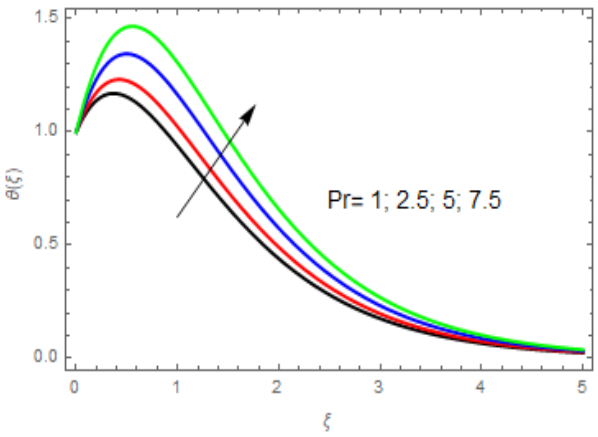

FIGURE 33. Impact of Pr on $\theta(\xi)$.

Figure 15 depicts the impact of Gr on h. The angular velocity rises through the Grashof number. An extremely fast-behavior within the entire boundary layer regime is monitored at angular velocity. Figure 16 shows the effect of m on $h(\xi)$. The Hall current parameter appears to be a double behavior within the flow of the fluid. The improvement in $h(\xi)$ can be seen nearer to the wall. In any case, for the whole part, the Hall current encourages the rotation of micro-elements. Figures 18 and 19 show the impact of Grc and K on $h(\xi)$. Figure 18 depicted the impact of Grc on $h(\xi)$, the increase in Grc reduces $h(\xi)$. Figure 19 shows the effect of K on $h(\xi)$, which shows that the greater value of K decreases $h(\xi)$ in all flow.

Figures 22 and 23 highlight the impact of some of the fluid parameters on the nanoparticle volume fraction profile. It is curious to note that the most extreme volume fraction is observed close to the channel walls, whereas the least volume fraction is found at the central level of the channel walls. Figure 22 shows that the increase in the Brownian motion parameter increases the nanoparticle volume fraction, while the increase in thermophoresis decreases the volume fraction profile of the fluid shown in Figure 23. This may be due to an increase in mass diffuseness. Figures 24 and 25 show the impact of the thermal radiation parameter and the Prandtl number on the volume fraction profile in nanoparticles, respectively. Figure 24 shows that the increase in the thermal radiation parameter increases the volume fraction within the fluid. Whereas, the increase in the number of Prandtl decreases this profile as shown in Figure 25. Figures 26 and 27 show the impact of the magnetic field parameter and the Reynolds number on the volume fraction profile, respectively. Figure 26 shows that an increase

TABLE 2. Influence of $M, m, \lambda,$ and K on $g'(0)$.

M	m	λ	K	$g'(0)$
0.1	1.1	1.1	0.3	0.012921
0.3				0.038763
0.5				0.064606
	1.2			0.059222
	1.3			0.054667
	1.4			0.050762
		1.2		0.049765
		1.3		0.047542
		1.4		0.045664
			0.4	0.052435
			0.5	0.059464
			0.6	0.068764

TABLE 3. Influence of $M, m, \lambda, N_b, N_t, R_d$ and Pr on $\theta'(0)$.

M	m	λ	Nb	Nt	Rd	Pr	$\theta'(0)$
0.1	1.1	1.1	0.1	0.3	0.2	0.72	0.577017
0.3							0.576611
0.5							0.576205
	1.2						0.576367
	1.3						0.576494
	1.4						0.576594
		1.2					0.576646
		1.3					0.489443
		1.4					0.424542
			0.2				0.480859
			0.3				0.471947
			0.4				0.463035
				0.4			0.454123
				0.5			0.445212
				0.6			0.436300
					0.3		0.499737
					0.4		0.566509
					0.5		0.636617
						1.0	0.647567
						5.0	0.803909
						10.0	0.999343

TABLE 4. Influence of A, Sc and Re on $\gamma'(0)$.

A	Sc	Re	$\gamma'(0)$
0.2	0.6	0.4	0.548838
0.4			0.569306
0.6			0.589773
	0.7		0.600007
	0.8		0.610240
	0.9		0.627407
		0.5	0.678657
		0.6	0.751186
		0.7	0.819075

in the magnetic field parameter decreases the volume fraction profile within the nanofluid, often due to the unstable impact of these parameters, which leads to the free flow of nanoparticles within the fluid, resulting in a decrease in the volume of nanoparticles. Figure 27 shows the effect of the Reynolds number on the volume fraction profile, showing from this figure that the increase in the Reynolds number increases the volume fraction towards the left wall and decreases towards the two walls due to the increase in the suction rate on the walls.

Figures 28 to 35 Present the impact of some dimensionless parameters on the temperature profile. Figure 27 shows that the increase in the magnetic field parameter reduces the temperature profile due to the introduction of the magnetic field, which weakens the hydrodynamic flow structure and reduces the heat transfer as it has a net positive effect. The effect of m on temperature profile $\theta(\xi)$ is shown in Figure 29. The temperature profile is consistently stimulated by the parameter Hall current. The reduction in boundary layer thickness is viewed. Figure 30 depicts the effect

TABLE 5. Influence of M, Gr, Grc, N_b, N_t, m, n, K, $N1$, Re, *and* Pr on C_{fx} and C_{fz}.

M	Gr	Grc	Nb	Nt	m	n	K	$N1$	Re	Pr	C_{fx}	C_{fx}
0.1											-2.29561	0.024639
0.4											-2.35942	0.098204
4.0											-3.21022	0.939679
	0.6										-2.26723	0.024658
	0.8										-2.21047	0.024698
	0.9										-2.18210	0.024718
		0.6									-2.43666	0.024541
		0.8									-2.49308	0.024502
		0.9									-2,52129	0.024483
			0.3								-2.40838	0.024561
			0.5								-2.40831	0.024561
			0.8								-2.40820	0.024561
				0.4							-2.40841	0.024561
				0.6							-2.40834	0.024561
				0.8							-2.40827	0.024561
					1.4						-2.28747	0.019368
					1.6						-2.28439	0.016950
					1.8						-2.28228	0.015069
						1.3					-3.61661	0.016651
						1.5					-3,78658	0.015922
						1.7					-3.95094	0.015275
							0.4				-2.41664	0.024437
							0.6				-2.43358	0.024188
							0.8				-2.45120	0.023939
								0.3			-2.42399	0.024550
								0.4			-2.43953	0.024539
								0.6			-2.47018	0.024518
									2.0		-1.07676	0.010984
									4.0		-0.76121	0.007767
									10.0		-0.48121	0.049122
										1.0	-2.40852	0.024561
										6.0	-2.40970	0.024561
										10.0	-2.41065	0.024561

of Gr on $\theta(\xi)$. Intensifying Grashof number reduces the thickness of the boundary layer and therefore shows a decrease in temperature. The impact of Br on q is shown in Figure 31, which shows the increase in temperature through Br. Figures 32 and 33 show the influence of the thermal radiation parameter and the Prandtl number on the temperature profile. It is obvious that the temperature decreases with an increase in the thermal radiation parameter as shown in Figure 32, which results in an increase in the rate of heat transfer; i.e. an increase in the convection cooling at the level of the right wall due to an increase in the loss of heat in the surrounding environment, which leads to a drop in the temperature of the micropolar nanofluid couple stress. Figure 33 shows that the increase in the Prandtls number increases the temperature of the fluid, since thermal phenomena dominate the hydrodynamic phenomenon due to the high Prandtls number. Figures 34 and 35 show the effect of the thermophoresis parameter and Brownian motion parameter on the temperature profile, respectively. It is noted that the temperature profile increases and the thickness of the thermal boundary layer increases in the presence of nanoparticles in terms of Brownian motion and

TABLE 6. Influence of M, Gr, Grc, N_b, N_t, m, n, K, $N1$, Re and Pr on Nu_x and Sh.

M	Gr	Grc	Nb	Nt	m	n	K	$N1$	Re	Pr	Nu_x	Sh
0.1											0.561011	0.492739
0.4											0.559825	0.492739
4.0											0.546105	0.492739
	0.6										0.561015	0.492739
	0.8										0.561023	0.492739
	0.9										0.561027	0.492739
		0.6									0.560999	0.492739
		0.8									0.560984	0.492739
		0.9									0.560981	0.492739
			0.3								0.555250	0.492739
			0.5								0.549509	0.492739
			0.8								0.540932	0.492739
				0.4							0.558183	0.492739
				0.6							0.552579	0.492739
				0.8							0.547004	0.492739
					1.4						0.561163	0.492739
					1.6						0.561220	0.492739
					1.8						0.561260	0.492739
						1.3					0.811483	0.709855
						1.5					0.846051	0.739873
						1.7					0.879260	0.768190
							0.4				0.560995	0.492739
							0.6				0.560992	0.492739
							0.8				0.560990	0.492739
								0.3			0.560994	0.492739
								0.4			0.560992	0.492739
								0.6			0.560987	0.492739
									2.0		1.254530	1.160440
									4.0		1.774280	1.705890
									10.0		2.805730	2.911060
										1.0	0.563696	0.492739
										6.0	0.612456	0.492739
										10.0	0.652206	0.492739

thermophoresis; due to the increase in the temperature gradient and the thermal and mass diffusion of the nanofluid, the heat fluid particles tend to migrate from the canal's hot zone to the cold zone. Furthermore, the local temperature in the thermal boundary layer increases as the effect of thermophoresis and Brownian motion increases. It can be inferred that nanoparticles can play a significant role in improving convection.

Table 1 show that, the effect of $M, N1, m, \lambda, Gr, Grc, N_f$, *and* K on $f''(0)$ *and* $g'(0)$. The higher the value of $M, Grc, K, N1$, and N_f the lower the value of $f''(0)$ along $x-axis$ which has direct effect to the skin friction, while Gr, λ and m have an opposite effect on the same $x-axis$. Table 2 revealed that, the higher the M and K, increases $g'(0)$ along the $z-axis$ where m and λ have an opposite effect on the same $z-axis$. Table 3 show the effects of $M, m, \lambda, N_b, N_t, \mathrm{R}_d$ and Pr on $\theta'(0)$ heat flux and Sh mass transfer. It is noted that the temperature increases by the increase of m, R_d and Pr while M, λ, N_b, N_t shown in the table decreases the temperature profile. Table 4 notice the influence of A, Sc and Re on volume fraction profile which influence the rate of mass transfer. The variation of the of dimensionless parameters on velocities profile displayed in Table 5 showing that, the effect of $M, Gr, Grc, N_b, N_t, m, n, K, N1$, Re and Pr on C_{fx} and C_{fz}. The higher the value of $M, Grc, n, K, N1$, Re

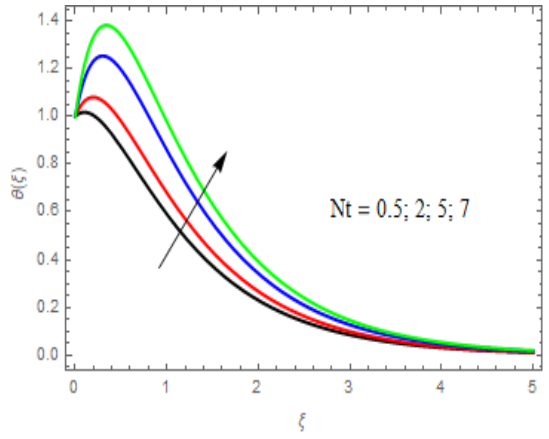

FIGURE 34. Impact of N_t on $\theta(\xi)$.

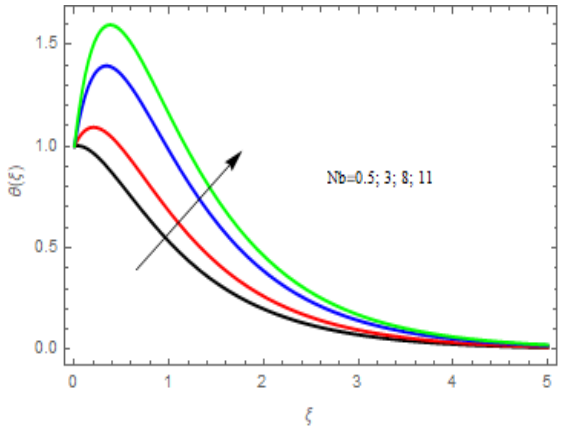

FIGURE 35. Impact of N_b on $\theta(\xi)$.

and Pr the rise in skin friction along $x-axis$ C_{fx} while Gr, Nb, Nt and m have an opposite effect on skin friction along $x-axis$ C_{fx}. The higher the $Grc, m, n, K, N1,$ and Re, the increase in skin friction along the $z-axis$ C_{fz} where M and Gr have an opposite effect on skin friction along the $z-axis$ C_{fz} and N_t, N_b and Pr has no impact on skin friction along the $z-axis$ C_{fz}. Table 6 show the effects of $M, Gr, Grc, N_b, N_t, m, n, K, N1$, Re and Pr on Nu_x heat flux and Sh mass transfer. It is noted that the heat flux increases by $Gr, m, n,$ and Pr, while the remaining parameters shown in the table decrease the heat flux. The table shows that the rate of mass transfer in relation to the left wall is improved at the level of the right wall.

Variations in $M, Gr, Grc, Nb, Nt, m, K, N1,$ and Pr do not influence the rate of mass transfer. This is rational since these parameters have no effect on the gradient of concentration, and do not appear in the concentration equation. Due to more nanofluid injection, the Sherwood number increases at the right side of the channel when the Reynolds number increases.

V. CONCLUSION

The paper presented a novel study of the more complex problem involving both heat and mass transfer in an incompressible micropolar nanofluid flow over a non-linear extended surface with magnetic parameters for double diffusion convection, Hall parameter, couple stress parameter, viscous dissipation, Brownian motion and thermophoresis parameters.

- Primary velocity with higher magnetic parameter, local Grashof number and Grashof solutal number decreases, while increasing with a couple stress parameter and Hall parameter.
- Secondary velocity increases with higher local Grashof number and Hall parameter, while it is decreases with higher couple stress parameter, magnetic parameter and Grashof solutal number.
- Angular velocity decreases with a higher magnetic parameter, a Grashof solutal number and a couple stress parameter, while increasing with a larger Hall parameter and a local Grashof number.
- The increase in the value of the solutary Grashof number implies an increase in the temperature of the wall, which makes the bond between the micropolar nanofluid weaker, the strength of the internal friction decreasing, the gravity becoming stronger enough.
- Increasing Prandtl number, thermophoresis and Brownian motion improves the temperature profile and facilitates heat transfer which indicates that the temperature in the fluid is strongly influenced by the velocity profile.
- The temperature decreases with a higher magnetic parameter, local Grashof number, Hall parameter, and thermal radiation, which leads to an increase in the rate of heat transfer.
- Double diffuse convection significantly improves heat and mass transfer. In the case of a couple stress micropolar nanofluid, the effect is more prominent than for a clear fluid.
- The concentration decreases with the higher value of the Schmidt number, which shows that the mass diffusivity decays.
- Increase of the magnetic field parameter reduces the volume fraction profile within the micropolar nanofluid, often due to the unstable impact of this parameter, which leads to the free flow of nanoparticles within the fluid, resulting in a decrease in the volume of nanoparticles.
- The skin friction increases with the increase in magnetic parameter along $z-axis$ and opposite along $x-axis$.
- An increasing in the magnetic parameter M gives a decreasing in the values of the velocities and Nusselt number, or an increasing in the values of the couple stress at the surface, temperature and concentration.
- The material parameter K has the same effects of magnetic field parameter on the values of the velocities, temperature, concentration and Nusselt number.
- The heat flux decreases when Brownian motion and thermophoresis parameters increase.
- The heat and mass transfer increase with an increase in the number of Reynolds.

CONFLICTS OF INTEREST

The authors declare that they have no competing interests.

ACKNOWLEDGMENT

This research was accomplished with the help of the Theoretical and Computational Science (TaCS) Center, Faculty of Science, KMUTT. The authors are obliged to the respectable referees for their important and fruitful comments to enhance the quality of this article.

REFERENCES

[1] M. Born, "Über die Beweglichkeit der elektrolytischen Ionen," *Zeitschrift für Physik*, vol. 1, no. 3, pp. 221–249, Jun. 1920.
[2] H. Grad, "Statistical mechanics, thermodynamics, and fluid dynamics of systems with an arbitrary number of integrals," *Commun. Pure Appl. Math.*, vol. 5, no. 4, pp. 455–494, Nov. 1952.
[3] S. C. Cowin, "The theory of polar fluids," *Adv. Appl. Mech.*, vol. 14, no. 276, p. 1974, 1974.
[4] A. Eringen, "Theory of micropolar fluids," *Indiana Univ. Math. J.*, vol. 16, no. 1, pp. 1–18, 1966.
[5] A. C. Eringen, "Simple microfluids," *Int. J. Eng. Sci.*, vol. 2, no. 2, pp. 205–217, May 1964.
[6] S. Macheret, M. Shneider, G. Candler, R. Moses, and J. Kline, "Magnetohydrodynamic power generation for planetary entry vehicles," in *Proc. 35th AIAA Plasmadyn. Lasers Conf.*, Jun. 2004, p. 2560.
[7] Y. Peng, Z. Lin, L. Zhao, C. Sha, R. Li, Y. Xu, B. Liu, and J. Li, "Analysis of liquid metal MHD wave energy direct conversion system," in *Proc. 18th Int. Offshore Polar Eng. Conf.*, Jan. 2008, p. 388.
[8] L. Hu, H. Kobayashi, and Y. Okuno, "Analyses on response of a liquid metal MHD power generation system to various external inputs," *IEEJ Trans. Electr. Electron. Eng.*, vol. 10, no. 3, pp. 268–273, May 2015.
[9] T. Hardianto, N. Sakamoto, and N. Harada, "Three-dimensional flow analysis in a faraday-type MHD generator," *IEEE Trans. Ind. Appl.*, vol. 44, no. 4, pp. 1116–1123, 2008.
[10] V. Rajesh, M. P. Mallesh, and O. A. Bég, "Transient MHD free convection flow and heat transfer of nanofluid past an impulsively started vertical porous plate in the presence of viscous dissipation," *Procedia Mater. Sci.*, vol. 10, pp. 80–89, Jan. 2015.
[11] T. Murakami and Y. Okuno, "High-density energy conversion using compact magnetohydrodynamic electrical power generator," *Appl. Phys. Lett.*, vol. 91, no. 16, Oct. 2007, Art. no. 161506.
[12] M. Farooq, S. Islam, M. T. Rahim, and T. Haroon, "Heat transfer flow of steady couple stress fluids between two parallel plates with variable viscosity," *Heat Transf. Res.*, vol. 42, no. 8, pp. 737–780, 2011.
[13] D. Srinivasacharya and K. Kaladhar, "Mixed convection flow of couple stress fluid in a non-Darcy porous medium with Soret and Dufour effects," *J. Appl. Sci. Eng.*, vol. 15, pp. 415–422, Dec. 2012.
[14] M. Ramzan, M. Farooq, A. Alsaedi, and T. Hayat, "MHD three-dimensional flow of couple stress fluid with newtonian heating," *Eur. Phys. J. Plus*, vol. 128, no. 5, p. 49, May 2013.
[15] J. C. Umavathi and M. S. Malashetty, "Oberbeck convection flow of a couple stress fluid through a vertical porous stratum," *Int. J. Non-Linear Mech.*, vol. 34, no. 6, pp. 1037–1045, Nov. 1999.
[16] T. Hayat, M. Mustafa, Z. Iqbal, and A. Alsaedi, "Stagnation-point flow of couple stress fluid with melting heat transfer," *Appl. Math. Mech.*, vol. 34, no. 2, pp. 167–176, Feb. 2013.
[17] M. Turkyilmazoglu, "Exact solutions for two-dimensional laminar flow over a continuously stretching or shrinking sheet in an electrically conducting quiescent couple stress fluid," *Int. J. Heat Mass Transf.*, vol. 72, pp. 1–8, May 2014.
[18] F. Awad, N. A. H. Haroun, P. Sibanda, and M. Khumalo, "On couple stress effects on unsteady nanofluid flow over stretching surfaces with vanishing nanoparticle flux at the wall," *J. Appl. Fluid Mech.*, vol. 9, no. 6, pp. 1937–1944, Jul. 2016.
[19] S. Sreenadh, S. N. Kishore, A. N. S. Srinivas, and R. H. Reddy, "MHD free convection flow of couple stress fluid in a vertical porous layer," *Adv. Appl. Sci. Res.*, vol. 2, no. 6, pp. 215–222, 2011.
[20] T. Hayat, M. Awais, A. Safdar, and A. A. Hendi, "Unsteady three dimensional flow of couple stress fluid over a stretching surface with chemical reaction," *Nonlinear Anal., Model. Control*, vol. 17, no. 1, pp. 47–59, 2012.
[21] N. A. Khan, S. Aziz, and N. A. Khan, "Numerical simulation for the unsteady MHD flow and heat transfer of couple stress fluid over a rotating disk," *PLoS ONE*, vol. 9, no. 5, 2014, Art. no. e95423.
[22] S. Rosseland, *Theoretical Astrophysics*. Oxford, U.K.: Clarendon press, 1936.
[23] A. S. Dogonchi and D. D. Ganji, "Analytical solution and heat transfer of two-phase nanofluid flow between non-parallel walls considering joule heating effect," *Powder Technol.*, vol. 318, pp. 390–400, Aug. 2017.
[24] A. S. Dogonchi, M. Alizadeh, and D. D. Ganji, "Investigation of MHD go-water nanofluid flow and heat transfer in a porous channel in the presence of thermal radiation effect," *Adv. Powder Technol.*, vol. 28, no. 7, pp. 1815–1825, Jul. 2017.
[25] A. S. Dogonchi and D. D. Ganji, "Study of nanofluid flow and heat transfer between non-parallel stretching walls considering brownian motion," *J. Taiwan Inst. Chem. Engineers*, vol. 69, pp. 1–13, Dec. 2016.
[26] A. S. Dogonchi, K. Divsalar, and D. D. Ganji, "Flow and heat transfer of MHD nanofluid between parallel plates in the presence of thermal radiation," *Comput. Methods Appl. Mech. Eng.*, vol. 310, pp. 58–76, Oct. 2016.
[27] E. Khodabandeh and A. Abbassi, "Performance optimization of water-Al_2O_3 nanofluid flow and heat transfer in trapezoidal cooling microchannel using constructal theory and two phase eulerian-lagrangian approach," *Powder Technol.*, vol. 323, pp. 103–114, Jan. 2018.
[28] A. S. Dogonchi and D. D. Ganji, "Effect of Cattaneo–Christov heat flux on buoyancy MHD nanofluid flow and heat transfer over a stretching sheet in the presence of joule heating and thermal radiation impacts," *Indian J. Phys.*, vol. 92, no. 6, pp. 757–766, Jun. 2018.
[29] A. S. Dogonchi and D. D. Ganji, "Thermal radiation effect on the nano-fluid buoyancy flow and heat transfer over a stretching sheet considering brownian motion," *J. Mol. Liquids*, vol. 223, pp. 521–527, Nov. 2016.
[30] A. S. Dogonchi and D. D. Ganji, "Impact of Cattaneo–Christov heat flux on MHD nanofluid flow and heat transfer between parallel plates considering thermal radiation effect," *J. Taiwan Inst. Chem. Engineers*, vol. 80, pp. 52–63, Nov. 2017.
[31] R. Mashayekhi, E. Khodabandeh, M. Bahiraei, L. Bahrami, D. Toghraie, and O. A. Akbari, "Application of a novel conical strip insert to improve the efficacy of water-Ag nanofluid for utilization in thermal systems: A two-phase simulation," *Energy Convers. Manage.*, vol. 151, pp. 573–586, Nov. 2017.
[32] S. Roseland, *Theoretical Astrophysics*. Oxford, U.K.: Clarendon press, 1936.
[33] M. N. Ozisik, *Radiative Transfer and Interactions With Conduction and Convection*. New York, NY, USA: Wiley, 1973, p. 587.
[34] R. Barzegarian, M. K. Moraveji, and A. Aloueyan, "Experimental investigation on heat transfer characteristics and pressure drop of BPHE (brazed plate heat exchanger) using TiO_2–water nanofluid," *Exp. Thermal Fluid Sci.*, vol. 74, pp. 11–18, Jun. 2016.
[35] R. Barzegarian, A. Aloueyan, and T. Yousefi, "Thermal performance augmentation using water based Al_2O_3-gamma nanofluid in a horizontal shell and tube heat exchanger under forced circulation," *Int. Commun. Heat Mass Transf.*, vol. 86, pp. 52–59, Aug. 2017.
[36] K. Hosseinzadeh, M. Alizadeh, and D. D. Ganji, "Hydrothermal analysis on MHD squeezing nanofluid flow in parallel plates by analytical method," *Int. J. Mech. Mater. Eng.*, vol. 13, no. 1, p. 4, Dec. 2018.
[37] Z. Shah, P. Kumam, A. Dawar, E. O. Alzahrani, and P. Thounthong, "Study of the couple stress convective micropolar fluid flow in a hall MHD generator system," *Frontiers Phys.*, vol. 7, p. 171, Nov. 2019, doi: 10.3389/fphy.2019.00171.
[38] O. A. Beg, M. Ferdows, M. E. Karim, M. M. Hasan, T. A. Bég, M. D. Shamshuddin, and A. Kadir, "Computation of non-isothermal thermo-convective micropolar fluid dynamics in a Hall MHD generator system with non-linear distending wall," *Int. J. Appl. Comput. Math.*, vol. 6, no. 2, Apr. 2020, Art. no. 42.
[39] S. J. Liao, *Beyond Perturbation: Introduction to Homotopy Analysis Method*. Boca Raton, FL, USA: CRC Press, 2003.